Preparation of glycopolymer-coated magnetite nanoparticles for hyperthermia treatment

ARTICLE *in* JOURNAL OF POLYMER SCIENCE PART A POLYMER CHEMISTRY · DECEMBER 2012

Impact Factor: 3.11 · DOI: 10.1002/pola.26367

5 AUTHORS, INCLUDING:

Gema Marcelo
University of Alcalá
30 PUBLICATIONS **297** CITATIONS
SEE PROFILE

Francisco Jose Teran
Madrid Institute for Advanced Studies
57 PUBLICATIONS **437** CITATIONS
SEE PROFILE

Marta Fernández-García
Spanish National Research Council
160 PUBLICATIONS **2,089** CITATIONS
SEE PROFILE

Preparation of Glycopolymer-Coated Magnetite Nanoparticles for Hyperthermia Treatment

Alexandra Muñoz-Bonilla,[1] Gema Marcelo,[1] Cintia Casado,[2] Francisco J. Teran,[2] Marta Fernández-García[1]

[1]Instituto de Ciencia y Tecnología de Polímeros (ICTP-CSIC), C/Juan de la Cierva 3, 28006-Madrid, Spain
[2]Instituto Madrileño de Estudios Avanzados en Nanociencia, IMDEA-Nanociencia,
Campus Universidad Autónoma de Madrid, Madrid 28049, Spain
Correspondence to: A. Muñoz-Bonilla (E-mail: sbonilla@ictp.csic.es)

Revised 17 August 2012; accepted 29 August 2012; published online 21 September 2012
DOI: 10.1002/pola.26367

ABSTRACT: In this article, magnetite nanoparticles (MNPs) coated with glycopolymer bearing glucose moieties were designed with optimal structural, colloidal, and magnetic properties for biomedical applications. MNPs with an average size of 17 ± 2 nm were synthesized by thermal decomposition process and then their surfaces were modified with active vinyl groups. Two different monomers were immobilized onto the surfaces: dopamine methacrylamide, a monomer with properties inspired on mussels adhesive capacity, or unprotected glycomonomer, 2-{[(D-glucosamin-2*N*-yl)carbonyl]-oxy}ethyl methacrylate. Afterward, the glycomonomer were polymerized at the interface of both vinyl functionalized MNPs by conventional radical polymerization. The resultant hybrid NPs were water dispersible presenting good stability in aqueous solution for long time periods. Moreover, the high density of carbohydrates at the surface of the magnetic NPs could confer targeting properties to the system as demonstrated by studies of their binding interactions with lectins, where the binding activity is higher as the glycopolymer content augments. The magnetic and magneto-thermal properties of the synthesized hybrid NPs were evaluated. The magnetization curves reveal superparamagnetic features at 300 K, with high values of saturation magnetization. Furthermore, the hybrid glycoparticles show suitable heat dissipation power when exposed to alternating magnetic field conditions. © 2012 Wiley Periodicals, Inc. J Polym Sci Part A: Polym Chem 50: 5087–5096, 2012

KEYWORDS: aqueous stability; dynamic light scattering; glycopolymers; hybrid nanoparticles; hyperthermia; magnetite nanoparticles; radical polymerization; thermal properties

INTRODUCTION Over the past decade magnetic iron oxide nanoparticles (NPs) have generated a great interest in the scientific community due to many high technology and promising applications such as terabit magnetic storage devices, catalysis, and sensors.[1] Furthermore, they are easily degraded and metabolized *in vivo* and their low toxicity[2] makes them suitable in separation and purification processes, or biomedicine applications such as drug delivery carriers,[3] contrast agents for magnetic resonance imaging (MRI),[4] or intracellular heating generators.[3,4] For the latest application, the control of the size,[5] the size distribution, crystallinity degree, and superparamagnetic features are required in order to dissipate heat in the presence of alternating magnetic fields.[6,7]

The crystallinity of the hydrophobic particles, arising from the high temperature synthesis, has been claimed to be one of the crucial parameters to obtain high-quality magnetic NPs, as compared to those synthesized by low-temperature coprecipitation methods.[8–10] Also, thermal decomposition processes affords the control over the size, the size dispersion, and the morphology of magnetite particles. Initially, they are poorly dispersed in aqueous solution due to their hydrophobic surface coatings; nevertheless they can be stabilized in aqueous media by simply ligand exchange extending their use in biomedicine.[11–14] Most of the biomedical applications require surface modifications of the magnetite nanoparticles (MNPs) in order to ensure their colloidal stability in aqueous medium, providing controlled aggregate size, biocompatible features, or active groups for anchoring linkers. To this respect, the surface of MNPs (Fe_3O_4 NPs) can be modified with different ligand such as dextran, poly(ethylene glycol), peptides, or carbohydrates.[15–18] Of particular interest is the combination of magnetic NPs and carbohydrate bioactivities since the latter play an important role in physiological and pathological recognition systems. The saccharides molecules are involved in many recognition events, principally on the cell membranes, through specific interactions with proteins such as enzymes or lectins, depending on the nature of the carbohydrate. These recognition processes are the initiating step in many biological functions based on cell–cell interactions such as cell growth regulation, cancer cell metastasis, or inflammation.[19–24] Therefore, due to their

biocompatibility and specific receptor recognition ability they have been extensively investigated for targeted drug and gene delivery applications.[25] Concerning the magnetic NPs, the decoration of the surface by carbohydrates provides not only dispersion of the particles in aqueous medium but also enables the uptake of the particles into the cells by endocytosis through lectin membrane-bounded receptors.[26,27] Recently, magnetic NPs bearing carbohydrate ligands have been synthesized to detect and differentiate cancer cells.[28] Moreover, the functionalization of the magnetic NPs with sugars could increase their affinity toward cancer cells. This is because sugars, mainly glucose and fructose, are the principal energy source of cells and in this sense cancer cells are well known to display an enhanced sugar uptake and consumption as compared with normal cells.[29]

Several examples of magnetic NPs bearing carbohydrate moieties have been reported in literature.[30–40] In this concern, the multivalent effect of densely packed saccharides, which is termed "glycoside clustering effect," could offer an important improvement of the target ability for recognition of these magnetic NPs. The carbohydrate–protein interaction is generally weak[41,42] and the glyco-cluster effect tremendously amplifies the binding affinity. Thus, the coating of magnetic NPs with glycopolymers should manifest an important enhancement of the target properties. Various methods have been developed to achieve functionalized surfaces with glycopolymers such as "grafting techniques,"[43–45] using glycopolymer surfactants[46] or the layer by layer assembly approach,[47] among others. However, only few examples can be found in literature with respect to magnetite NPs functionalized with glycopolymers. Modification of magnetite surface with glycopolymers or carbohydrate units have been carried out after coating magnetite surface, mainly with silica or gold.[26,35–40] Besides, glycosylated poly(pentafluorostyrene) has been physically adsorbed onto magnetic NPs.[48] However and to the best of our knowledge, no examples dealing with polymerization at the interfaces to coat covalently the magnetite surface with a glycopolymer shell have been reported.

Dopamine, 4-(2-aminoethyl)-benzene-1,2-diol, is known as brain neurotransmitters but also is an essential components of the mussel adhesive protein. In the last years, there has been an increasing interest in the development of new adhesive materials based on this catechol chemistry, which allows the rapid and strong adhesion of these adhesives onto the surface of metal oxides such as TiO_2, Al_2O_3, and Fe_3O_4.[49–52] It has been demonstrated that poly(ethylene glycol) (PEG) appended with different catechol molecules is strongly adhered to magnetite surface and allows the transference to aqueous media.[53] Therefore, catechol chemistry affords new via to magnetite surface modification in order to obtain biocompatibility, biofouling, and biofunctional surfaces.[54] In this article, we explore the adhesive properties of a methacrylamide monomer bearing dopamine in its structure to be bond covalently to magnetite surface and to further form a glycopolymer coating by polymerization at the interface. These modified magnetite NPs will be used as seeds of the radical polymerization of a glycomonomer bearing glucose moieties to form glycopolymer decorating the magnetite surface. Moreover, a second approach is also investigated based on the adhesive properties of the glycomonomer itself. In addition, the large amount of glycosylated units endows the targeting function to be recognized for specific proteins.

EXPERIMENTAL

Materials

Iron (III) acetylacetonate, oleic acid, dibenzyl ether, sodium hydroxide (NaOH), hydrochloric acid (HCl), and triethylamine (TEA) were all purchased from Aldrich and used as received. The unprotected glycomonomer, 2-{[(D-glucosamin-2-*N*-yl)carbonyl]oxy}ethyl methacrylate (HEMAGl) was synthesized according to the procedure described previously.[55] The dopamine methacrylamide (DMA) was prepared and characterized according to a modified method[56] based on a previously reported strategy.[57] 2,2′-Azobisisobutyronitrile, AIBN (Fluka), was purified by successive crystallizations from methanol. Tetrahydrofuran (THF), ethanol (EtOH), and dimethylformamide (DMF) were purchased from Scharlau. Lectin-fluorescein isothiocyanate conjugate from *Canavalia ensiformis* (Con A-FITC) was supplied by Sigma-Aldrich. The buffer trizma-HCl was pursued from Aldrich and sodium chloride (NaCl; Panreac), manganese chloride tetrahydrate, ($MnCl_2$ $4H_2O$; 99%, Fluka), calcium chloride dihydrate ($CaCl_2$ $2H_2O$; 99.5%, Fluka) were added for the molecular recognition.

Synthesis of Magnetite Nanoparticles

Oleic acid-functionalized MNPs were prepared according to previously described work.[8] In a typical synthesis, iron (III) acetylacetonate (0.71 g) was added to a mixture of oleic acid (1.13 g) and benzyl ether (15.02 g). The mixture solution was degassed at room temperature for 1 h and then, was heated to 200°C for 2 h, and stirred under a flow of argon gas. The mixture was heated to reflux, 298 °C, for 60 min in the same flow of argon gas. The reaction mixture was maintained at this temperature for 120 min. After cooling to room temperature, a mixture of toluene and hexane was added to the solution. The solution was centrifuged to precipitate the Fe_3O_4 NPs. The separated precipitate was washed several times using chloroform.

Functionalization of Magnetite with DMA and HEMAGl

A biomimetic coating strategy has been chosen to modify the magnetite surface. That is, the oleic acid coating the pristine magnetite surface was exchanged by DMA. In a parallel approach, the glycomonomer was immobilized into the surface by displacement of the oleic acid. The oleic acid-stabilized Fe_3O_4 NPs (15 mg) were dispersed in 3 mL of DMF and 250 mg of either DMA or HEMAGl were added to the mixture. The dispersion was treated with a sonifier (1 h, settings: 20% amplitude, 3 s on and 2 s off). The particles were isolated with an external magnetic field and were rinsed with EtOH at least three times. Fourier transform infrared spectroscopy (FTIR) and X-ray photoelectron

spectra (XPS) were measured to characterize the magnetite surface.

Polymerization of HEMAGl on Magnetite Particle Surface (Fe_3O_4@Glycopolymer NPs)

The glycopolymer coating on the MNPs were realized by conventional radical polymerization of HEMAGl from both vinyl modified Fe_3O_4 NPs (with DMA or HEMAGl). In a typical polymerization, 13.5 mg of Fe_3O_4 NPs covered with DMA or HEMAGl were placed into a round bottom flask and dispersed in 10 mL of DMF by ultrasonic treatment. Vigorous magnetic stirring was applied to form a homogeneous medium. Then 340 mg of HEMAGl were added to the dispersion, the mixture was stirred vigorously, and bubbled with argon for 15 min. After the addition of 5 mg of AIBN into the dispersion the reaction was allowed to proceed at 80 °C for 4 h. The Fe_3O_4@glycopolymer NPs were isolated with an external magnetic field and, subsequently, washed several times with DMF and ethanol.

Molecular Recognition

The MNPs coated with glycopolymer (1 mg), Fe_3O_4@DMA-glycopolymer or Fe_3O_4@HEMAGl-glycopolymer NPs, were incubated with 2 mL of a buffer solution (Trizma, pH 7.4, with 1 mM $MnCl_2$, 1 mM $CaCl_2$, and 0.1 M NaCl) containing 1 mg of Con A-FITC. After the incubation the particles were attracted to the wall of the recipient with an external magnetic field. The supernatant were separated and analyze by fluorescence spectroscopy.

Measurements

Transmission electron microscopy (TEM) images were obtained from JEOL JEM-2100 TEM instrument (with a LaB_6 filament, operating voltage = 200 kV). Scanning electron microscopy (SEM) measurements were performed using field emission scanning electron microscope (FE-SEM) (Hitachi, SU 8000, Japan) at 5 kV in transmitted electron imaging mode. The samples for both TEM and FE-SEM were prepared from a dispersion of magnetite particles or glycopolymer-coated magnetite particles in hexane or EtOH, respectively, which was dropped onto a carbon-coated copper grid. The particle size distributions were performed using the image analysis software (ImageJ, http://rsb.info.nih.gov/ij/). XPS were recorded with a VG Escalab 200 R spectrometer equipped with a hemispherical electron analyzer and an Mg Kα ($h\nu$ = 1253.6 eV) non-monochromatic X-ray source. The samples were degassed in the pretreatment chamber at room temperature for 1 h prior to being transferred into the instrument's ultra-high vacuum analysis chamber. The spectra were calibrated in relation to the C 1 s binding energy (284.6 eV), which was applied as an internal standard. X-ray diffraction (XRD) patterns were recorded in the reflection mode by using a Bruker D8 Advance diffractometer provided with a PSD Vantec detector (from Bruker, Madison, WI). Cu Kα radiation (λ = 0.1542 nm) was used, operating at 40 kV and 40 mA. The parallel beam optics was adjusted by a parabolic Göbel mirror with horizontal grazing incidence Soller slit of 0.12° and LiF monochromator. The equipment was calibrated with different standards. A step scanning mode was employed for the detector. The diffraction scans were collected within the range of 2θ = 4–80°, with a 2θ step of 0.024° and 0.5 s per step. The hydrodynamic diameter of each NP sample in solution (0.11 mg/mL in Millipore water) was determined by dynamic light scattering (DLS) using a Malvern Zetasizer Nano ZS series equipment. NP dispersions were sonicated for 10 min and left to equilibrate for 2 min before the measurements. FTIR spectra of KBr pellets were recorded using a Perkin Elmer Spectrum 2000 FTIR spectrometer incorporating a deuterated triglycine sulfide (DTGS) detector and an extended range KBr beamsplitter. Thermogravimetric analyses (TGA) were carried out on a TGA Q500-0885 equipment of TA Instrumental Analysis. Dynamic experiments were performed at a heating rate of 10 °C/min from room temperature up to 800 °C under nitrogen atmosphere. The specific interaction of Con A-FITC with the glycopolymer–MNPs were studied by fluorescence spectroscopy and recorded on a Perkin–Elmer LS50B spectrophotometer using excitation light of 470 nm. The field dependence of the magnetization for the particles was obtained using a superconducting quantum interface device magnetometer (SQUID, Quantum Design, MPMS-XL) operated at 300 K. Calorimetry measurements of glycopolymer-coated MNPs under non-adiabatic conditions were performed in a home-made set-up of reduced sample volume (<40 μL).[58] The sample holder is a glass flask with a vacuum shield covered by a polystyrene stopper where an upper aperture allows us to introduce the temperature probe. Alternating magnetic field (H_{AC}) up to 250 kHz and 50 mT are generated by a home-made air-cooled ferrite core coiled with Litz wires, which is part of a LCR resonant circuit. The temperature was measured with a commercial optical fiber probe TS2/2 connected to a FOTEMP2-16 two-channel signal conditioner from Optocon AG with an experimental error of ±0.2 °C. For this study, calorimetry measurements have been performed on a reduced volume (30 μL) of NPs dispersed in water for two iron concentration of 4 and 8 g/L. NPs were subjected to H_{AC} with different frequencies (from 40 to 200 kHz) and amplitudes (from 10 to 50 mT) for 8 min under thermal equilibrium temperatures around 25 °C.

RESULTS AND DISCUSSION

Synthesis of the Oleic Acid Capped Fe_3O_4 NPs (Fe_3O_4@oleic acid NPs)

MNPs coated with oleic acid were synthesized via thermal decomposition process with controllable size and uniform shape. The size and size distribution are in turn affected by the synthetic route, and this was designed to tailor a size below 20 nm. For most of the biomedical applications the preferred size of the NPs is typically around 10–20 nm, where each particle becomes a single domain showing superparamagnetic behavior. The TEM micrograph shows well-defined cube shaped structures with a mean uniform edge length of 17 ± 2 nm (Figure 1).

Vinyl Modification of the Fe_3O_4 NPs

The functionalization of the Fe_3O_4 NPS with vinyl groups was carried out by displacement of oleic acid molecules with either

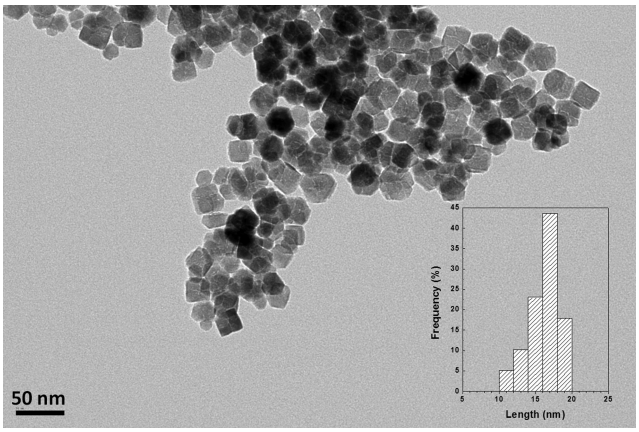

FIGURE 1 TEM images of the synthesized Fe_3O_4 NPs coated with oleic acid. (Inset) Size distribution histogram obtained from the micrograph.

DMA or HEMAGl (Scheme 1). The ligand exchange was achieved by mixing a DMF solution of DMA or HEMAGl and Fe_3O_4@oleic acid NPs in DMF and sonication. Although the non-covalent attachment of the carbohydrates to the magnetite surface contrary to the dopamine containing monomers, the high amount of hydroxyl groups per molecule stabilize the NPs[46] and can potentially displace the oleic acid molecules.

FTIR spectra of the magnetite NPS before and after the ligand exchange with either DMA or HEMAGl are displayed in Figure 2. The FTIR spectrum of Fe_3O_4@oleic acid NPs is dominated by a strong absorption band at 574 cm^{-1} attributed to the Fe—O deformation in octahedral and tetrahedral sites. The characteristic bands of the oleyl chains at 2923 cm^{-1} (asymmetric C—H stretch), 2853 cm^{-1} (symmetric C—H stretch), 1627 cm^{-1} (asymmetric COO^- stretch), and 1395 cm^{-1} (asymmetric COO^- stretch) are also appreciated. After the modification of the surface with DMA or HEMAGl, the characteristic band at 1395 cm^{-1} of oleic acid remarkably decreased, whereas additional peaks appear, consistent with the vibration modes of DMA, that is, an absorption band centered at 1635 cm^{-1} assigned to the C—C vibration of catechol rings.

Moreover to confirm the success of the surface modification of the MNPs with active vinyl groups, the chemical composition of the NPs were further investigated via XPS. This technique is particularly useful to characterize surface coating, giving information not only of the chemical composition but also about the chemical states. In the survey spectrum of the Fe_3O_4@DMA NPs, Figure 3, mainly C, O, N, and Fe are identified as expected. The detection of the nitrogen signal at 402 eV clearly points out the successful immobilization DMA onto the magnetite surface. In addition, the Fe2p spectrum shows the typical structure for iron oxides with a broad doublet peak ($Fe2p_{3/2}$ and $Fe2p_{1/2}$). Moreover, the absence of the signal around 719 eV which is typical for maghemite seems to evidence that the Fe_3O_4 NPs after dopamine modification remain with the same chemical structure, magnetite, and no oxidation to maghemite is observed.[59] Concerning the Fe_3O_4@HEMAGl NPs, almost a similar survey spectrum was detected as displayed in Figure 3. The nitrogen signal at 402 eV corroborates again the modification of the magnetite surface with the glycomonomer, HEMAGl. The Fe2p spectrum reveals along with the absence of the signal at 719 eV, the appearance of a low-binding energy in the peak at 711 eV indicates that the chemical structure of the NPs surface is magnetite and, consequently, no oxidation has taken place during the ligand exchange.

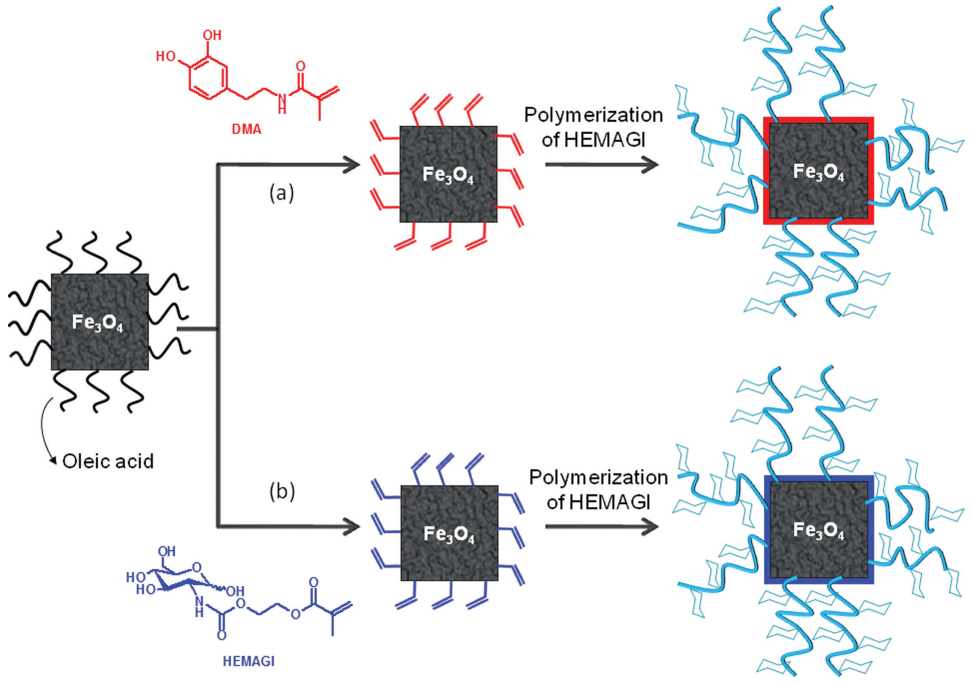

SCHEME 1 Vinyl modification of Fe_3O_4 NPs with DMA or HEMAGl and posterior polymerization of HEMAGl.

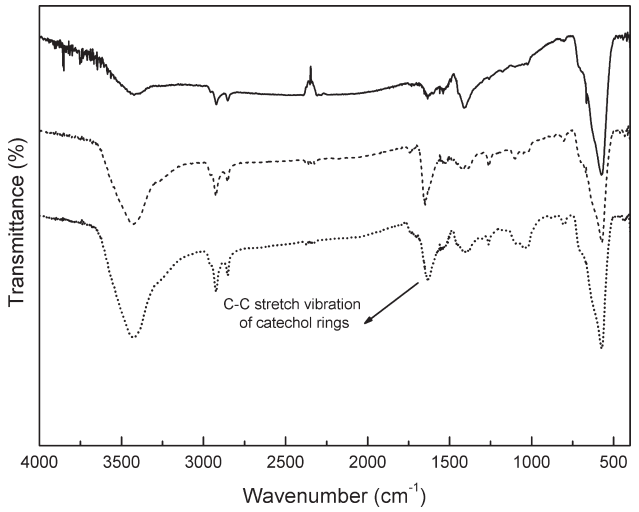

FIGURE 2 FTIR spectra of (—) Fe_3O_4@oleic acid NPs, (---) Fe_3O_4@DMA NPs, and (···) Fe_3O_4@HEMAGI NPs.

Preparation of Fe_3O_4@glycopolymer Hybrid NPs

According to the FTIR and XPS measurements, the DMA and HEMAGl monomers are successfully attached to the magnetite surfaces. Hence, in the following step, the radical polymerization of the glycomonomer HEMAGl is done in the presence of these functionalized NPs in order to form a glycopolymer shell around the Fe_3O_4 NPs. The C=C double bond from the surface-capped monomers would copolymerize with growing PHEMAGl radicals anchoring of the glycopolymer onto Fe_3O_4 NPs. The radical polymerization of HEMAGl was carried out in a DMF dispersion of the glycomonomer and the vinyl modified Fe_3O_4 NPs, with a weight monomer/NPs ratio of 25/1. After the polymerization from both seed NPs (Fe_3O_4@DMA and Fe_3O_4@HEMAGl NPs), the presence of the glycopolymer on the surface of the NPs was verified by FTIR, as can be seen in Figure 4. In comparison with the spectra of the Fe_3O_4 NPs coated with vinyl groups, after polymerization, it can be clearly observed two strong C=O stretching vibration bands at 1704 and 1633 cm^{-1} attributed to the ester and carbamate groups, respectively, of

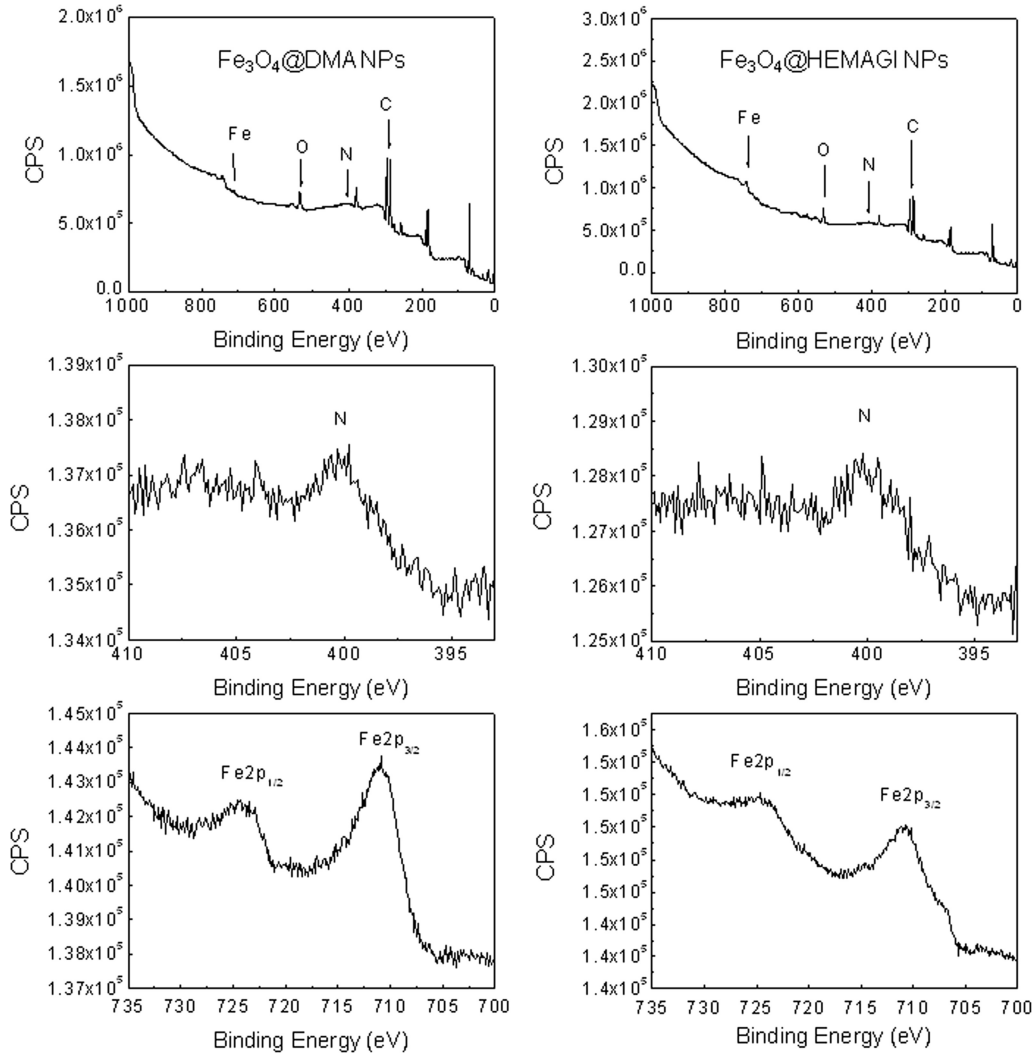

FIGURE 3 Selected XPS spectra of the Fe_3O_4@DMA and Fe_3O_4@HEMAGl NPs.

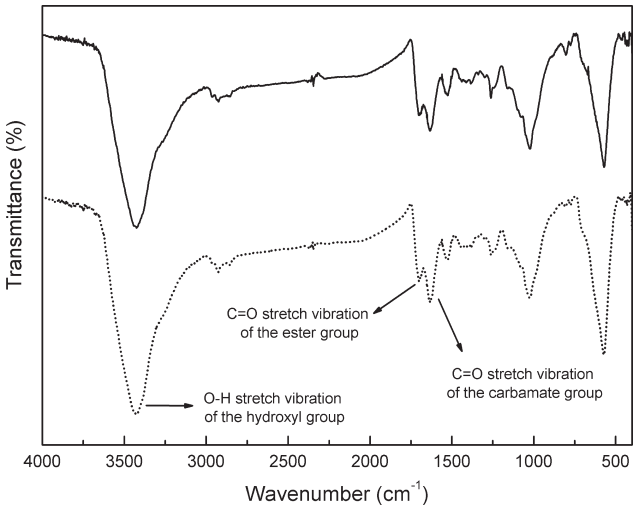

FIGURE 4 FTIR spectra of Fe_3O_4@glycopolymer NPs obtained from (···) Fe_3O_4@DMA NPs and (—) Fe_3O_4@HEMAGl NPs.

the polymerized glycomonomer units. Moreover, the broad absorption band at 3400 cm^{-1} corresponds to the hydroxyl group of the carbohydrates units.

Then, TGA was carried out to quantify the glycopolymer grown around the Fe_3O_4 NPs. The analysis revealed that the Fe_3O_4@glycopolymer NPs obtained from DMA coated particles (Fe_3O_4@DMA-glycopolymer NPs) have a 21 wt % of glycopolymer, whereas those prepared from the particles capped with the glycomonomer HEMAGl (Fe_3O_4@HEMAGl-glycopolymer NPs) result in a 28 wt % (Fig. 5). The reason for this relatively higher conversion achieved from the particles modified with the glycomonomer could be due to the relative reactivity of monomer pairs. In the case of NPs with DMA, probably the copolymerization of HEMAGl and DMA is less favorable than the HEMAGl homopolymerization where the rate of homopropagation in the case of HEMAGl could be higher than the rate of cross-propagation.

The glycopolymer shell of Fe_3O_4 NPs was clearly visualized by FE-SEM for both Fe_3O_4@glycopolymer hybrid NPs systems as depicted in Figure 6. The glycopolymer layer (light gray area) appeared on the coated magnetite core (dark black area) with average thickness around 20 nm.

DLS analysis in aqueous solution was performed to measure the average size of synthesized Fe_3O_4@DMA-glycopolymer and Fe_3O_4@HEMAGl-glycopolymer NPs. It is important to remark long-term stability of the MNPs coated with glycopolymer which remain dispersed and stable in aqueous solution contrary to the vinyl modified Fe_3O_4@DMA or Fe_3O_4@HEMAGl NPs before the polymerization. Besides the glycosylated particles redisperse well by simple mixing and sonication. Figure 7(a) shows the intensity average particle size distribution for Fe_3O_4@DMA-glycopolymer NPs, exhibiting two distinct particle size distributions. The peaks observed around 75 nm could be attributed to the individual NPs, while the dominant peaks are ascribed to the scattering of larger aggregates. On the other hand, number average particle size distribution displayed in Figure 7(b) shows that the dominant peak in this case is the one corresponding to the individual NPs. This observation is explained by the higher scattering intensity of large aggregates compared to small aggregates. This DLS size is consistent with that estimated through the FE-SEM images (Fig. 6), taking into account the hydrodynamic radius including the solvated layer of the glycopolymer, whereas in FE-SEM measurements this layer is collapsed. Similar results were also observed for the Fe_3O_4@HEMAGl-glycopolymer NPs.

Molecular Recognition Ability

Subsequently, FITC conjugated Concanavalin A (Con A), a specific lectin for binding glucose and mannose residues, was used to study the interaction between the lectin and the glucose moieties on the surface of magnetic NPs. To this purpose, the fluorescently labeled Con A was incubated with the Fe_3O_4@glycopolymer hybrid NPs in a buffer solution. Then, the application of an external magnetic field to the sample would remove the fluorescent lectin from the solution, if the NPs bind with the lectin. As a consequence the fluorescent intensity of the supernatant would be reduced. Figure 8 shows that the incubation during 30 min of the Con A-FITC (0.5 mg/mL) with only 0.5 mg/mL of Fe_3O_4@glycopolymer NPs followed by magnetic separation led to a significant reduction of the solution emission intensity. Therefore, the glycopolymer shell attached to the MNPs maintains the biological recognition capability. This reduction of the emission intensity is much higher in the case of Fe_3O_4@HEMAGl-glycopolymer NPs, up to 88% in comparison with the Fe_3O_4@DMA-glycopolymer NPs that only diminishes 69%. These results are consistent with the TGA measurements where the weight percentage of glycopolymer was quantified, indicating a higher amount of glycopolymer in the polymerization from the Fe_3O_4@HEMAGl seed NPs. Consequently, it can be concluded that the lectin–NPs interactions increase with the glycopolymer percentage.

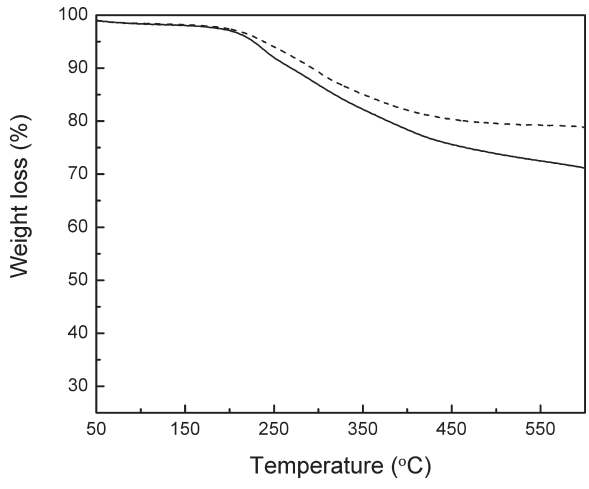

FIGURE 5 TGA of Fe_3O_4@glycopolymer NPs obtained from (---) Fe_3O_4@DMA NPs and (—) Fe_3O_4@HEMAGl NPs.

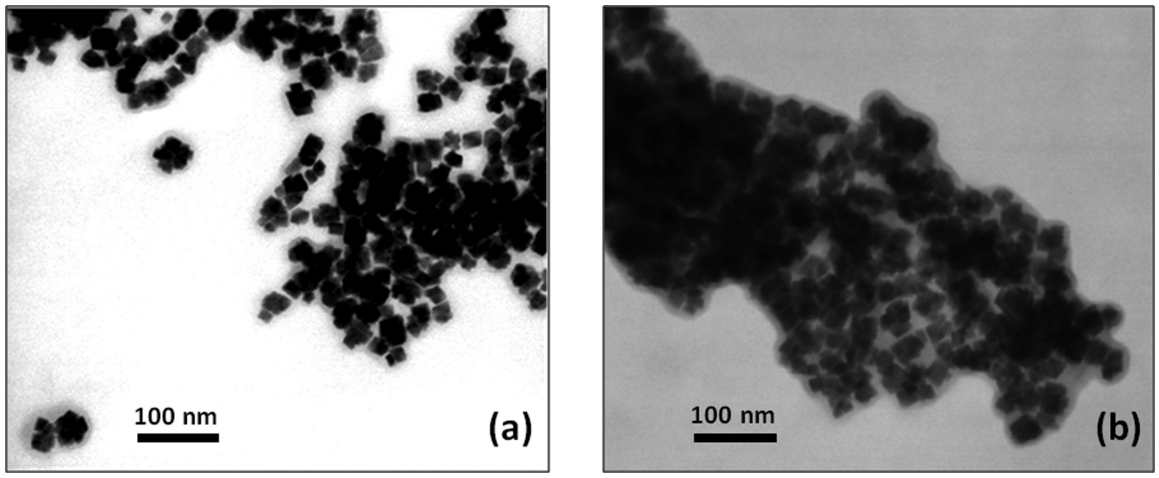

FIGURE 6 FE-SEM micrograph of (a) Fe_3O_4@HEMAGl-glycopolymer NPs and (b) Fe_3O_4@DMA-glycopolymer NPs.

XRD measurements of the magnetic NPs coated with glycopolymer were performed to investigate the polymorphism of the magnetic particles after the formation of the glycopolymer shell around the particles, whether or not they retain the magnetite form. The X-ray diffractogram for Fe_3O_4@HEMAGl-glycopolymer NPs is shown in Figure 9. All of the diffraction peaks are consistent with the database in JCPDS file (PCPDFWIN v.2.02, PDF No. 85-1436), and could be indexed according to the inverse spinel structure of magnetite. This result reveals that the MNPs do not suffer any oxidation to maghemite after the polymerization of HEMAGl. It is well known that magnetite is preferred in ferrofluids over maghemite because of their greater saturation magnetization. In the following section, the magnetic properties of the synthesized glycopolymer-MNPs will be discussed in order to evaluate their potential for hyperthermia applications.

Magnetic Properties

The magnetization measurements at 300 K of the glycopolymer-coated MNPs are shown in Figure 10. Oleic acid-functionalized MNPs show high saturation magnetization values (75 emu/g). Although the expected decrease in saturation magnetization after polymer coating, the hybrid magnetic glycoparticles still retained excellent magnetization. The saturation magnetization values of Fe_3O_4@HEMAGl-glycopolymer and Fe_3O_4@DMA-glycopolymer are 51 and 57 emu/g, respectively. The lower value obtained for the Fe_3O_4@HEMAGl-glycopolymer NPs is due to the larger proportion of glycopolymer around the NPs as compared with the Fe_3O_4@DMA-glycopolymer NPs. Considering only the magnetic NP core, about 72% and 79% in weight, their values are, approximately, 71 and 72 emu/g for Fe_3O_4@HEMAGl-glycopolymer and Fe_3O_4@DMA-glycopolymer, which indicates again that the magnetite nature remains practically unchanged.[60]

Furthermore, the magnetic studies for all the samples show almost no hysteresis loops in the magnetization curves at 300 K with negligible coercivity (~1.1 mT) and magnetization remanence (1 emu/g) at zero magnetic fields, reflecting

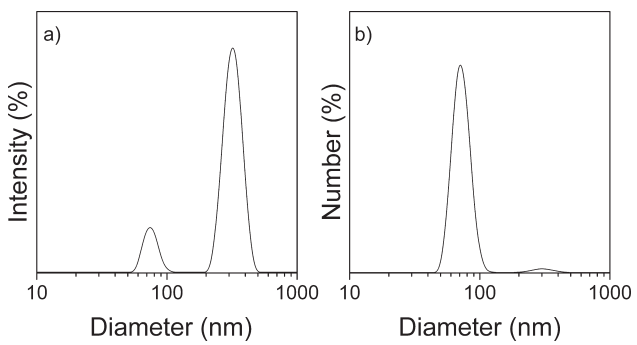

FIGURE 7 (a) Intensity average size distribution and (b) number average size distribution for the Fe_3O_4@DMA-glycopolymer NPs in water solution.

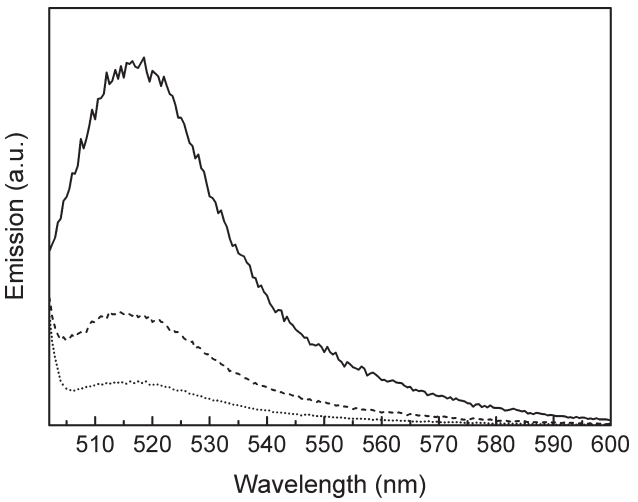

FIGURE 8 Fluorescent emission intensities of supernatants of (—) Con A-FITC (0.5 mg/mL) and Con A-FITC upon incubation with (---) Fe_3O_4@DMA-glycopolymer NPs (0.5 mg/mL) and (···) Fe_3O_4@HEMAGl-glycopolymer NPs (0.5 mg/mL), both followed by magnet-mediated isolation ($\lambda_{excitation} = 470$ nm).

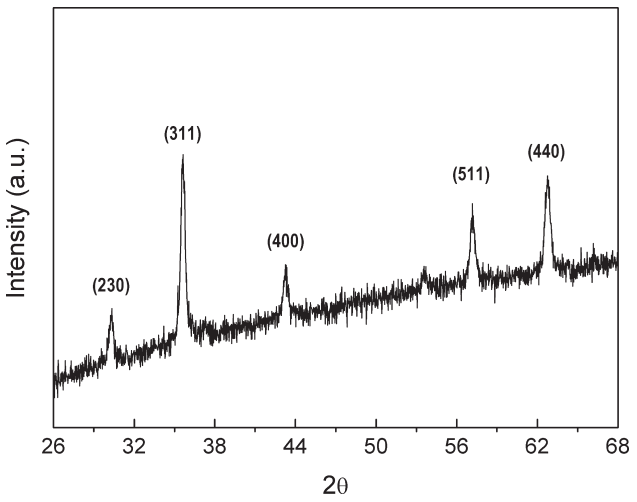

FIGURE 9 XRD patterns of the Fe_3O_4@HEMAGl-glycopolymer NPs.

the superparamagnetic features of Fe_3O_4 NPs as expected for their size (17 nm), smaller than single magnetic domain.[58]

Calorimetry Measurements

When magnetite NPs are exposed to alternating magnetic fields (H_{AC}) at suitable frequency and amplitude conditions, heat dissipation is observed due to Néel and/or Brownian mechanisms.[61] This is clearly reflected in the increase of the NP temperature when H_{AC} is turned on. In order to determine the specific absorption rate (SAR) of the glycopolymer-coated magnetite NPs, calorimetry measurements were performed under H_{AC} and non-adiabatic conditions at equilibrium temperatures near 25 °C. Figure 11 shows the temperature variation with time of Fe_3O_4@DMA-glycopolymer NPs for an iron concentration of 8 g/L when subjected to 72 kHz and 25 mT for 8 min. At first glance, a sudden hybrid NPs temperature increase is observed when H_{AC} is turned on (gray zone) followed by a progressive temperature stabilization at longer times. Finally, hybrid NPs temperature decays when H_{AC} is turned off (white zone) due to heat losses transferred to the surrounding. In order to extract mass-normalized SAR values, the temperature variation curves of NPs proved in an experimental set-up of controlled heat losses was simulated.[62] Thus, SAR values showed typical superparamagnetic behavior, increasing with the frequency (see inset plot of Fig. 11) from 10 to 50 W/g when frequency varies from 40 to 200 kHz at constant field amplitude of 25 mT. These SAR values are not far from the ones which have successfully employed in intracellular hyperthermia studies leading to significant shrinking of the cell viability after H_{AC} exposure.[63]

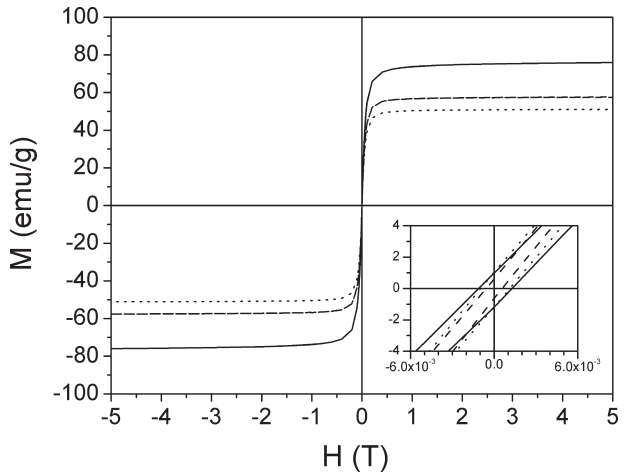

FIGURE 10 Squid magnetization cycles at 300 K of (—) Fe_3O_4@oleic acid NPs and Fe_3O_4@glycopolymer NPs obtained from (---) Fe_3O_4@DMA NPs and (···) Fe_3O_4@HEMAGl NPs.

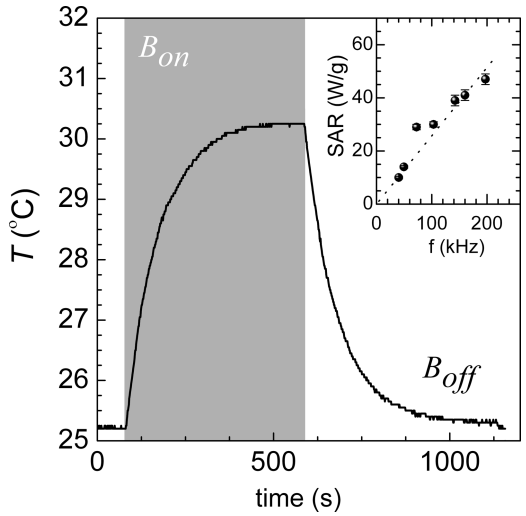

FIGURE 11 Time evolution of Fe_3O_4@DMA-glycopolymer NPs's temperature at 8 g/L subjected to H_{AC} (72 kHz and 25 mT). Inset: frequency dependence of SAR for Fe_3O_4@DMA-glycopolymer NPs at 8 g/L.

Although the Fe_3O_4@HEMAGl-glycopolymer NPs present a larger proportion of glycopolymer around the NPs as compared with the Fe_3O_4@DMA-glycopolymer NPs, they show similar SAR values at given H_{AC} conditions. Furthermore, the mass-normalized SAR values obtained for hybrid NPs at given H_{AC} conditions are similar for concentrations ranging from 4 to 8 g/L. These obtained values are consistent with other candidate systems based on carbohydrate coatings reported in the literature.[5]

CONCLUSIONS

Hybrid MNPs coated with glycopolymers are developed by a simple and effective method. The resulting hydrophobic and crystalline MNPs obtained by thermal decomposition process are modified at their surface by ligand exchange of oleic acid by DMA or HEMAGl monomers, introducing in this way vinyl functionality to the surfaces. Then, radical polymerization of the glycomonomer is carried out in the presence of the MNPs and the glycopolymer shell around them is formed. The amount of glycopolymer attached to the particles is larger when the polymerization is performed from the

glycomonomer-coated magnetic NPs (Fe_3O_4@HEMAGl NPs). Moreover, the carbohydrates moieties of the glycopolymer layer retain their biological recognition capability, which is higher as the content of glycopolymer increases on the NPs. It is also demonstrated that after formation of the hydrophilic shell, the MNPs are dispersible in water, without affecting their shape or their magnetic properties. The heat dissipation power of the MNPs when subjected to alternating magnetic fields confirms their potential capabilities for intracellular hyperthermia applications.

ACKNOWLEDGMENTS

This work was partially supported by Spanish Ministry of Economy and Competitiveness (MAT2010-17016 and MAT2010-21822-C02-01). G. Marcelo, A. Muñoz-Bonilla, and F.J. Teran acknowledge financial support from JAE-doc CSIC grants, Juan de la Cierva and Ramon y Cajal (RYC-2011-09617) subprograms, respectively.

REFERENCES AND NOTES

1 Frey, N. A.; Peng, S.; Cheng, K.; Sun, S. *Chem. Soc. Rev.* **2009,** *38*, 2532–2542.

2 Gupta, A. K.; Gupta, M. *Biomaterials* **2005,** *26*, 3995–4021.

3 Mejías, R.; Pérez-Yagüe, S.; Gutiérrez, L.; Cabrera, L. I.; Spada, R.; Acedo, P.; Serna, C. J.; Lázaro, F. J.; Villanueva, A.; Morales, M. P.; Barber, D. F. *Biomaterials* **2011,** *32*, 2938–2952.

4 Lu, A. H.; Salabas, E. L.; Schüth, F. *Angew. Chem. Int. Ed.* **2007,** *46*, 1222–1244.

5 Lartigue, L.; Innocenti, C.; Kalaivani, T.; Awwad, A.; Sanchez Duque, M. M.; Guari, Y.; Larionova, J.; Guérin, C.; Montero, J.-L. G.; Barragan-Montero, V.; Arosio, P.; Lascialfari, A.; Gatteschi, D.; Sangregorio. C. *J. Am. Chem. Soc.* **2011,** *133*, 10459–10472.

6 Kumar, C. S.; Mohammad. F. *Adv. Drug Deliv. Rev.* **2011,** *63*, 789–808.

7 Mehdaoui, B.; Meffre, A.; Carrey, J.; Lachaize, S.; Lacroix, L. M.; Gougeon, M.; Chaudret, B.; Respaud, M. *Adv. Funct. Mater.* **2011,** *21*, 4573–4581.

8 Guardia, P.; Batlle-Brugal, B.; Roca, A. G.; Iglesias, O.; Morales, M. P.; Serna, C. J.; Labarta, A.; Batlle, X. *J. Magn. Magn. Mater.* **2007,** *316*, E756–E759.

9 Roca, A. G.; Marco, J. F.; Morales, M. D.; Serna, C. J. *J. Phys. Chem. C* **2007,** *111*, 18577–18584.

10 Kim, D.; Lee, N.; Park, M.; Kim, B. H.; An, K.; Hyeon, T. *J. Am. Chem. Soc.* **2009,** *131*, 454–455.

11 Roca, A. G.; Costo, R.; Rebolledo, A. F.; Veintemillas-Verdaguer, S.; Tartaj, P.; González-Carreño, T.; Morales, M. P.; Serna, C. J. *J. Phys. D: Appl. Phys.* **2009,** *42*, 224002–224012.

12 Nan, A.; Turcu, R.; Craciunescu, I.; Pana, O.; Scharf, H.; Liebscher, J. *J. Polym. Sci. Part A: Polym. Chem.* **2009,** *47*, 5397–5404.

13 Nan, A.; Turcu, R.; Liebscher, J. *J. Polym. Sci. Part A: Polym. Chem.* **2012,** *50*, 1485–1490.

14 Karsten, S.; Nan, A.; Turcu, R.; Liebscher, J. *J. Polym. Sci. Part A: Polym. Chem.* **2012**, *50*, 3986–3995.

15 Xie, J.; Chen, K.; Lee, H.-Y.; Xu, C.; Hsu, A. R.; Peng, S.; Chen, X.; Sun, S. *J. Am. Chem. Soc.* **2008,** *130*, 7542–7543.

16 Medeiros, S. F.; Santos, A. M.; Fessi, H.; Elaissari, A. *Int. J. Pharm.* **2011,** *403*, 139–161.

17 Yang, J.; Lee, T. I.; Lim, E.-K.; Hyung, W.; Lee, C.-H.; Song, Y. J.; Suh, J.-S.; Yoon, H.-G.; Huh, Y.-M.; Haam, S. *Chem. Mater.* **2007,** *19*, 3870–3876.

18 Tassa, C.; Shaw, S. Y.; Weissleder, R. *Acc. Chem. Res.* **2011,** *44*, 842–852.

19 Mengerink, K. J.; Vacquier, V. D. *Glycobiology* **2001,** *11*, 37R–43R.

20 Takasaki, S.; Mori, E.; Mori, T. *Biochim. Biophys. Acta Gen. Subj.* **1999,** *1473*, 206–215.

21 Geijtenbeek, T. B.; Kwon, D. S.; Torensma, R.; van Vliet, S. J.; van Duijnhoven, G. C.; Middel, J.; Cornelissen, I. L.; Nottet, H. S.; Kewal-Ramani, V. N.; Littman, D. R.; Figdor, C. G.; van Kooyk, Y. *Cell* **2000,** *100*, 587–597.

22 Tirrell, D. A. *Nature* **2004,** *430*, 837–837.

23 Lowe, J. B.; Marth, J. D. *Annu. Rev. Biochem.* **2003,** *72*, 643–691.

24 Ohtsubo1, K.; Marth, J. D. *Cell* **2006,** *126*, 855–867.

25 Zhang, H.; Ma, Y.; Sun, X.-L. *Med. Res. Rev.* **2010,** *30*, 270–289.

26 Barragan, V.; Menger, F. M.; Caran, K.; Vidil, C.; Morere, A.; Montero, J.-L. *Chem. Commun.* **2001,** *1*, 85–86.

27 Ahmed, M.; Lai, B. F. L.; Kizhakkedathu, J. N.; Narain, R. *Bioconjug. Chem.* **2012,** *23*, 1050–1058.

28 El-Boubbou, K.; Zhu, D. C.; Vasileiou, C.; Borhan, B.; Prosperi, D.; Li, W.; Huang, X. *J. Am. Chem. Soc.* **2010,** *132*, 4490–4499.

29 Blanco Calvo, M.; Figueroa, A.; Grande Pulido, E.; García Campelo, R.; Antón Aparicio, L. *Int. J. Endocrinol.* **2010,** article ID 205357.

30 Shimomura, M.; Ono, B.; Oshima, K.; Miyauchi, S. *Polymer* **2006,** *47*, 5785–5790.

31 El-Boubbou, K.; Gruden, C.; Huang, X. *J. Am. Chem. Soc.* **2007,** *129*, 13392–13393.

32 Horák, D.; Babic, M.; Jendelová, P.; Herynek, V.; Trchová, M.; Pientka, Z.; Pollert, E.; Hájek, M.; Syková, E. *Bioconjug. Chem.* **2007,** *18*, 635–644.

33 Lartigue, L.; Oumzil, K.; Guari, Y.; Larionova, J.; Guérin, C.; Montero, J.-L.; Barragan-Montero, V.; Sangregorio, C.; Caneschi, A.; Innocenti, C.; Kalaivani, T.; Arosio, P.; Lascialfari, A. *Org. Lett.* **2009,** *11*, 2992–2995.

34 Kekkonen, V.; Lafreniere, N.; Ebara, M.; Saito, A.; Sawa, Y.; Narain, R. *J. Magn. Magn. Mater.* **2009,** *321*, 1393–1396.

35 de la Fuente, J. M.; Alcántar, D.; Penadés, S. *IEEE Trans. Nanobiosci.* **2007,** *6*, 275–281.

36 Gallo, J.; García, I.; Padro, D.; Arnaiz, B.; Penadés, S. *J. Mater. Chem.* **2010,** *20*, 10010–10020.

37 Gallo, J.; García, I.; Genicio, N.; Padro, D.; Penadés, S. *Biomaterials* **2011,** *32*, 9818–9825.

38 García, I.; Gallo, J.; Genicio, N.; Padro, D.; Penadés, S. *Bioconjug. Chem.* **2011,** *22*, 264–273.

39 Pfaff, A.; Schallon, A.; Ruhland, T. M.; Majewski, A. P.; Schmalz, H.; Freitag, R.; Müller, A. H. E. *Biomacromolecules* **2011,** *12*, 3805–3811.

40 Gallo, J.; Genicio, N.; Penadés, S. *Adv. Healthcare Mater.,* **2012,** *1*, 302–307.

41 Lee, Y. C.; Lee, R. T. *Acc. Chem. Res.* **1995,** *28*, 321–327.

42 Miura, Y.; Ikeda, T.; Wada, N.; Sato, H.; Kobayashi, K. *Green Chem.* **2003,** *5*, 610–614.

43 Mateescu, A.; Ye, J.; Narain, R.; Vamvakaki, M. *Soft Matter* **2009,** *5*, 1621–1629.

44 Yang, Q.; Tian, J.; Hu, M.-X.; Xu, Z.-K. *Langmuir* **2007,** *23*, 6684–6690.

45 Housni, A.; Cai, H.; Liu, S.; Pun, S. H.; Narain, R. *Langmuir* **2007,** *23*, 5056–5061.

46 Muñoz-Bonilla, A.; Heuts, J. P. A.; Fernández-García, M. *Soft Matter* **2011,** *7*, 2493–2499.

47 Boyer, C.; Bousquet, A.; Rondolo, J.; Whittaker, M. R.; Stenzel, M. H.; Davis, T. P. *Macromolecules* **2010,** *43*, 3775–3784.

48 Babiuch, K.; Wyrwa, R.; Wagner, K.; Seemann, T.; Hoeppener, S.; Becer, C. R.; Linke, R.; Gottschaldt, M.; Weisser, J.; Schnabelrauch, M.; Schubert, U. S. *Biomacromolecules* **2011,** *12*, 681–691.

49 Lee, H.; Dellatore, S. M.; Miller, W. M.; Messersmith, P. B. *Science* **2007,** *318*, 426–430.

50 Xu, C.; Xu, K.; Gu, H.; Zheng, R.; Liu, H.; Zhang, X.; Guo, Z.; Xu, B. *J. Am. Chem. Soc.* **2004,** *126*, 9938–9939.

51 Waite, J. H. *Nat. Mater.* **2008,** *7*, 8–9.

52 Ye, Q.; Zhou, F.; Liu, W. *Chem. Soc. Rev.* **2011,** *40*, 4244–4258.

53 Amstad, E.; Gillich, T.; Bilecka, I.; Textor, M.; Reimhult, E. *Nano Lett.* **2009,** *9*, 4042–4048.

54 Na, H. B.; Palui, G.; Rosenberg, J. T.; Ji, X.; Grant, S. C.; Mattoussi. H. *ACS Nano* **2012,** *6*, 389–399.

55 León, O.; Bordegé, V.; Muñoz-Bonilla, A.; Sánchez-Chaves, M.; Fernández-García, M. *J. Polym. Sci. Part A: Polym. Chem.* **2010,** *48*, 3623–3631.

56 Ham, H. O.; Liu, Z.; Lau, K. H. A.; Lee, H.; Messersmith, P. B. *Angew. Chem. Int. Ed.* **2011,** *50*, 732–736.

57 Lee, H.; Lee, B. P.; Messersmith, P. B. *Nature* **2007,** *448*, 338–342.

58 Krishnan, K. M.; Pakhomov, A. B.; Bao, Y.; Blomqvist, P.; Chun, Y.; Gonzales, F.; Griffin, K.; Ji, X.; Roberts, B. K. *J. Mater. Sci.* **2006,** *41*, 793–815.

59 Grosvenor, A. P.; Kobe, B. A.; Biesinger, M. C.; McIntyre, N. S. *Surf. Interface Anal.* **2004,** *36*, 1564–1574.

60 Marcelo, G.; Pérez, E.; Corrales, T.; Peinado, C.; *J. Phys. Chem. C,* **2011,** *115*, 25247–25256.

61 Fortin, J. P.; Wilhelm, C.; Servais, J.; Ménager, C.; Bacri, J. C.; Gazeau, F. *J. Am. Chem. Soc.* **2007,** *129*, 2628–2635.

62 Teran, F. J.; Casado, C.; Mikuszeit, N.; Salas, G.; Bollero, A.; Morales, M. P.; Camarero, J. Miranda, R. *Appl. Phys. Lett.* **2012,** *101*, 062413–062416.

63 Asin, L.; Ibarra, M. R.; Tres, A.; Goya, G. F. *Pharm. Res.* **2012,** *29*, 1319–1327.